Available online at www.sciencedirect.com
SCIENCE DIRECT
International Journal of Multiphase Flow 32 (2006) 643–660
International Journal of Multiphase Flow
www.elsevier.com/locate/ijmulflow

A DNS study of laminar bubbly flows in a vertical channel

Jiacai Lu, Souvik Biswas, Gretar Tryggvason *

Worcester Polytechnic Institute, Mechanical Engineering Department, Worcester, MA 01609, United States

Received 11 November 2005; received in revised form 6 February 2006

Abstract

Direct numerical simulations are used to examine laminar bubbly flows in vertical channels. For equal size nearly spherical bubbles the results show that at steady state the number density of bubbles in the center of the channel is always such that the fluid mixture there is in hydrostatic equilibrium. For upflow, excess bubbles are pushed to the walls, forming a bubble rich wall-layer, one bubble diameter thick. For downflow, bubbles are drawn into the channel center, leading to a wall-layer devoid of bubbles, of a thickness determined by how much the void fraction in the center of the channel must be increased to reach hydrostatic equilibrium. The void fraction profile can be predicted analytically using a very simple model and the model also gives the velocity profile for the downflow case. For the upflow, however, the velocity increase across the wall-layer must be obtained from the simulations. The slip velocity of the bubbles in the channel core and the velocity fluctuations are predicted reasonably well by results for homogeneous flows.

Keywords: Bubbly flow; Direct numerical simulations; Two-fluid model

1. Introduction

Bubbly flows in vertical pipes and channels are encountered in a wide variety of industrial systems. The best-known early study of such flows is by Serizawa et al. (1975) who examined the void fraction distribution and the velocity profile in turbulent air–water bubbly flows. Other investigations include experiments by Wang et al. (1987), Liu and Bankoff (1993), Nakoryakov et al. (1981, 1996), Liu (1997), Kashinsky and Randin (1999), So et al. (2002), Guet et al. (2004), and Matos et al. (2004). Although there are some differences between the results obtained by the different investigators, possibly due to different bubble sizes, all show that for nearly spherical bubbles the void fraction distribution and the velocity profile in the core of the channel are relatively uniform and that a void fraction peak is generally found near the wall for upflow but not for downflow. Sufficiently deformable bubbles, on the other hand, show exactly the opposite behavior and migrate to the center of the channel in upflow and toward the walls in downflow. A number of authors have also developed two-fluid models of bubbly flows in vertical channels. General descriptions of the two-fluid model can be

* Corresponding author. Tel.: +1 508 831 5759; fax: +1 508 831 5680.
E-mail address: gretar@wpi.edu (G. Tryggvason).

0301-9322/$ - see front matter © 2006 Elsevier Ltd. All rights reserved.
doi:10.1016/j.ijmultiphaseflow.2006.02.003

found in Delhay (1982), Kataoka and Serizawa (1989), Zhang and Prosperetti (1994) and Drew and Passman (1999), for example. For a recent discussion of the development of averaging theories for even more complex situations, see Sirignano (2005). One of the earliest models for a turbulent flow in a vertical channel was developed by Drew and Lahey (1982) who solved the resulting equations using asymptotic analysis. The model reproduced the general trends seen experimentally, including uniform velocity and void fraction in the core, wall peaking for upflow and a wall-layer without bubbles for downflow. Subsequent investigators have solved the resulting equations numerically, see, e.g., Lopez-De-Bertodano et al. (1987, 1994), Kuo et al. (1997), and Guet et al. (2005). The model results generally reproduce the experimental results reasonably well. Extensions of the two-fluid model to handle non-uniform bubble size distributions can be found in Politano et al. (2003) and Celik and Gel (2002).

While the flow is likely to be turbulent in most cases of practical interest, laminar flow is an important limiting case that can be used to explore aspects of multiphase flow modeling that do not depend on the specifics of the turbulence. This was recognized by Antal et al. (1991) who developed a two-fluid model for such flows and compared the model predictions with experimental results. The agreement between the model and the experiments was good, although for upflow there is a need to introduce a wall repulsion force to keep the center of the bubbles at least a radius away from the walls and the authors observed some dependency on the exact value of the lift coefficient used. Other studies of laminar flow include the experimental investigation by Song et al. (2001) who studied flows with both uniform and non-uniform distribution of bubble sizes and Luo et al. (2003) who examined the motion of light particles. Both studies were done for upflow and wall peaking was found in both cases.

The model of Antal et al. (1991) was studied analytically by Azpitarte and Buscaglia (2003) who made the very important observation that the fluid in the center region of the channel is always in hydrostatic equilibrium. Biswas, Esmaeeli and Tryggvason (2005) conducted direct numerical simulations of two-dimensional bubbly flows and compared their results with the model Antal et al. Since the simulations assumed two-dimensional flow, Biswas et al. had to adjust the model parameters, but they found that once the parameters had been adjusted for one case, the model predicted other situations reasonably well.

In this paper we report a numerical study of bubbly flow at relatively modest Reynolds numbers where the channel flow is laminar in the absence of bubbles. The buoyancy driven motion of spherical bubbles in a vertical channel flow has a particularly simple structure, making it the natural place to start examining multiphase flow in confined geometries. The averaged motion of the liquid can, in particular, be described analytically for downflow and ''nearly'' analytically for upflow. We start by giving a summary of the analytical description, in Section 2.

2. Problem set-up

We consider the flow sketched in Fig. 1. The channel is vertical, of width W, and gravity points downward so the bubbles rise relative to the liquid. The imposed pressure gradient is selected to generate upflow in the left frame and downflow for the frame on the right. Here, and in what follows, we use a coordinate system where the cross-stream (or wall-normal) coordinate is x, the streamwise coordinate is y, and z is perpendicular to the flow and parallel to the walls.

The lift force on a clean spherical bubble rising in a vertical shear flow is directed toward the side where the fluid moves faster past the bubble, in a frame of reference moving with the bubble. In channels, where the fluid velocity is zero at the walls, the bubbles will therefore move laterally toward the walls for upflow and away from the walls in downflow. The average mixture density depends on the number density of bubbles, so the lateral motion increases the density of the mixture losing bubbles and decreases it where the bubbles are accumulating. For upflow the imposed pressure gradient that drives the flow has to be larger than the weight of the mixture and the excess pressure gradient is balanced by the shear force in the mixture. As bubbles are driven to the walls, from the middle of the channel, eventually the mixture density increases to a point where the weight of the mixture is balanced by the pressure gradient. The shear therefore becomes zero and the lateral migration of the bubbles stops. Similarly, for downflow the pressure gradient forces the flow downward but as the bubbles are driven away from the walls the mixture density in the middle of the channel decreases until the mixture is buoyant enough to match the pressure gradient and the shear in the middle becomes zero. Thus, for both upflow and downflow

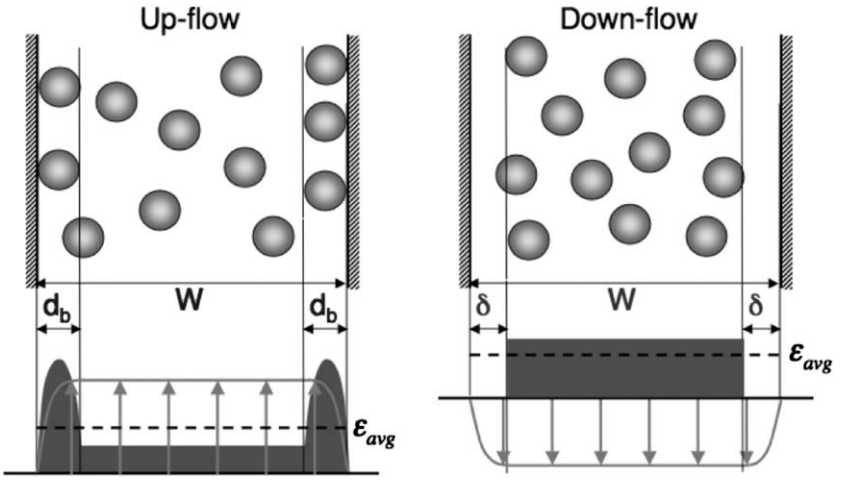

Fig. 1. A sketch of the structure of buoyancy driven bubbly flow in a vertical channel. In both cases the bubbles rise upward, but the direction of the fluid flow is different. In the frame on the left the flow is upward and in the frame on the right it is downward.

lateral migration of the bubbles changes the mixture density in the middle of the channel until the shear is zero and further lateral migration of the bubbles is stopped. For upflow the result is a bubble rich layer near the walls but for downflow the wall-layer is depleted of bubbles. The steady state void fraction and velocity profiles are shown schematically in Fig. 1. The profiles in both cases are obviously stable. If too many bubbles move to the wall in the upflow case, the mixture in the middle becomes sufficiently dense to overcome the pressure gradient and starts to fall down. This generates a shear that drives the bubbles out of the wall-layer, reducing the density in the middle again. In the same way, if too many bubbles accumulate in the middle of the channel, the mixture starts to rise by buoyancy, thus creating a shear that drives the bubbles back toward the wall. Similar considerations show that the downflow is also stable.

The simple structure of the flow allows us to derive a relatively straightforward mathematical description. Indeed, for the downflow case we can write down a complete solution without any adjustable parameters. For the upflow, however, we need to know the relation between the wall shear and the flow rate in the presence of bubbles.

A force balance on an elementary control volume in the channel at steady state gives

$$\frac{\mathrm{d}}{\mathrm{d}x}\tau(x) - \frac{\mathrm{d}p}{\mathrm{d}y} - \rho(x)g = 0, \tag{1}$$

where $\tau(x)$ is the shear stress, the second term is the imposed pressure gradient and the last term is the weight of the mixture. The direction of the flow is given by the sum of the pressure gradient and weight of the mixture, or by the sign of $\beta = \mathrm{d}p/\mathrm{d}y + \rho_{\mathrm{av}}g$. For $\beta < 0$ the pressure gradient overcomes the weight of the mixture and the flow is upward, but $\beta > 0$ results in downflow. The local density depends on the void fraction, $\rho = \varepsilon\rho_{\mathrm{G}} + (1-\varepsilon)\rho_{\mathrm{L}}$, and the average density, ρ_{av}, and the average void fraction, $\varepsilon_{\mathrm{av}}$, are related by $\rho_{\mathrm{av}} = \varepsilon_{\mathrm{av}} = \rho_{\mathrm{G}} + (1-\varepsilon_{\mathrm{av}})\rho_{\mathrm{L}}$. The subscripts G and L refer to the gas and the liquid, respectively. We can therefore rewrite (1) as

$$\frac{\mathrm{d}}{\mathrm{d}x}\tau(x) - \beta - g\Delta\rho(\varepsilon_{\mathrm{av}} - \varepsilon(x)) = 0, \tag{2}$$

where $\Delta\rho = \rho_{\mathrm{L}} - \rho_{\mathrm{G}}$. If there is no shear in the center of the channel, the void fraction in the center, ε_{c}, must be given by

$$\varepsilon_{\mathrm{c}} = \varepsilon_{\mathrm{av}} + \frac{\beta}{g\Delta\rho}. \tag{3}$$

For upflow ($\beta < 0$) the void fraction in the center will therefore be less than $\varepsilon_{\mathrm{av}}$, but for downflow ($\beta > 0$), the void fraction in the center will be larger than $\varepsilon_{\mathrm{av}}$. For upflow, the void fraction in the center becomes zero if the

pressure gradient is sufficiently large so that all the bubbles are driven to the wall and the discussion below is therefore limited to upflow cases where $\varepsilon_{av} + \beta/g\Delta\rho > 0$. For downflow the only limitation is that the void fraction in the center obviously cannot be larger than unity (very high void fraction approaching unity would likely result in bubble coalescence and violate the assumptions of small, nearly spherical bubbles).

For downflow the increase in void fraction in the center leads to a bubble free zone near the walls. The thickness of this zone is found by mass conservation: $\varepsilon_{av}W = \varepsilon_c(W - 2\delta)$. Using Eq. (3) and solving for the thickness of the wall-layer gives

$$\delta = \frac{\beta W}{2(\beta + \varepsilon_{av} g\Delta\rho)}. \tag{4}$$

Since there are no bubbles near the wall, the shear is given by $\tau = \mu_L(\mathrm{d}v/\mathrm{d}x)$ and the velocity can be found by integrating

$$\mu_L \frac{\mathrm{d}^2 v}{\mathrm{d}x^2} = \beta + \Delta\rho g \varepsilon_{av} \tag{5}$$

with the boundary conditions $u = 0$ at $x = 0$ and $\mathrm{d}v/\mathrm{d}x = 0$ at $x = \delta$. The velocity in the wall-layer is therefore

$$v(x) = \frac{(\beta + \varepsilon_{av} g\Delta\rho)}{2\mu_L}(x^2 - 2\delta x). \tag{6}$$

The velocity in the middle is uniform and can be found by taking $x = \delta$ in Eq. (6):

$$v_c = \frac{-\beta^2 W^2}{8\mu_L(\beta + \varepsilon_{av} g\Delta\rho)}. \tag{7}$$

The volume flux in the wall layer is $Q_\delta = \int_0^\delta v(x)\mathrm{d}x = -(\beta + \varepsilon_{av} g\Delta\rho)\delta^3/3\mu_L$ (since there are no bubbles in the wall layer) and the total liquid volume flux is

$$Q = \int_0^W (1-\varepsilon)v_L(x)\mathrm{d}x = 2Q_\delta + v_c(w - 2\delta)(1 - \varepsilon_c) = -\frac{(\beta W)^3}{8\mu_L(\beta + \varepsilon_{av} g\Delta\rho)^2}\left[\frac{2}{3} - \varepsilon_{av} + \frac{\Delta\rho g}{\beta}(1 - \varepsilon_{av})\right]. \tag{8}$$

For upflow, experimental results for nearly spherical bubbles generally show that the thickness of the wall peak is about a bubble diameter (e.g., Serizawa et al., 1975; Luo et al., 2003; Guet et al., 2005). Assuming the layer to be exactly equal to d_b, we can use mass conservation, $\varepsilon_{av}W = \varepsilon_c(W - 2d_b) + \varepsilon_w 2d_b$, and Eq. (3) to show that the average void fraction in the wall-layer is

$$\varepsilon_w = \varepsilon_c - \frac{W}{2d_b}\frac{\beta}{g\Delta\rho} = \varepsilon_{av} - \frac{\beta}{g\Delta\rho}\left(\frac{W}{2d_b} - 1\right). \tag{9}$$

Since $\beta < 0$, the wall-layer void fraction is higher than the average void fraction. The velocity in the wall-layer is more complex than for the downflow case because of the presence of the bubbles. We will not attempt to establish the relationship here, but instead defer a detailed discussion to a later paper.

For both the upflow and the downflow, the wall shear must balance the net pressure gradient at steady state:

$$2\tau_w = -\beta W. \tag{10}$$

This relationship, together with a constant flow rate, will be used below to check whether the flow is at steady state.

Notice that the motion of the bubbles plays essentially no part in the discussions above, except in determining the density of the mixture. The relative velocity of the bubbles, their dispersion and the unsteady liquid motion depends, of course, on the void fraction, but these quantities are essentially decoupled from the average motion of the liquid.

The flow in the channel is characterized by a Reynolds number that can, however, be defined in several ways. Here we use a Reynolds number based on a hypothetical parabolic velocity profile driven by the total pressure gradient β. Thus, we define a reference velocity $U_{ref} = \beta W^2/12\mu_L$. The half-width of the channel is used as a reference length, $L_{ref} = W/2$. The bubble motion is determined by the ratio of buoyancy and viscos-

Table 1
The parameters used in the simulations

Case	Downflow	Upflow	Upflow 2
Domain size	$1.6\times2\times0.5$	$1.5\times2\times0.5$	$2\times2\times0.5$
Resolution	$210\times256\times64$	$210\times256\times64$	$210\times256\times64$
Density ratio (ρ_G/ρ_L)	0.1	0.1	0.1
Viscosity ratio (μ_G/μ_L)	0.1	0.1	0.1
Pressure gradient ($\beta/g\Delta\rho$)	−0.032	0.04672	0.03115
Diameter of bubbles	0.2	0.2	0.16
Number of bubbles	40	44	60
Average void fraction in the whole channel	0.10472	0.12287	0.06434
Void fraction in hydrostatic equilibrium	0.13672	0.07615	0.03318
Eotvos number	0.5	0.5	0.5
Archimedes number	2000	2000	316.2
Reynolds number	2400	3504	721.2

ity, given by the Archimedes number, N, and although we will consider only nearly spherical bubbles, the shear near the walls is generally high and bubble deformability, governed by the Eötvös number, E_0, may play some role. In addition, we need to specify the average void fraction ε_{av}, and the relative importance of the pressure gradient and buoyancy, $\beta/g\Delta\rho$. The governing non-dimensional numbers are therefore:

$$Re_{ch}=\frac{\rho_L\beta W^3}{24\mu_L^2};\quad N=\frac{\rho_L^2 d_e^3 g}{\mu_L^2};\quad Eo=\frac{g\rho_L d_e^2}{\sigma};\quad \frac{\beta}{\Delta\rho g};\quad \varepsilon_{av}$$

In what follows, we shall limit our considerations to systems with bubbles of only one size. These non-dimensional numbers for each simulation discussed are listed in Table 1. Time is non-dimensionalized by $\tau_{ref}=L_{ref}/U_{ref}$, flow rate is normalized by $U_{ref}2L_{ref}$ and Reynolds stresses are normalized by $\beta W/2$.

3. Numerical method

The numerical method used for the simulations described in the next section is the finite volume/front tracking method introduced by Unverdi and Tryggvason (1992). The method has been described in detail by Tryggvason et al. (2001) and various validation studies can be found in Esmaeeli and Tryggvason (1999) and Bunner and Tryggvason (2002), for example. The Navier–Stokes equations are solved for the whole flow field, including both the liquid and the gas using a regular structured grid and the bubbles surface is tracked by an unstructured surface grid. The surface grid is used to determine the density and viscosity fields at each time step and to compute the surface tension. The method, with various improvements, has been used to study many aspects of bubbly flows, including the free buoyant rise of many bubbles (Esmaeeli and Tryggvason, 1998, 1999, 2005; Bunner and Tryggvason, 2002, 2003) Here, we use an implementation where the advection terms are computed using the non-conservative form and a QUICK scheme (Lu et al., 2005).

4. Results

The discussion in Section 2, along with Fig. 1, shows that there is a fundamental difference between the void fraction distribution in a channel with upflow and one where the liquid is flowing downward. We therefore start by examining two simulations, one for downflow and the other for upflow, where the set-up is similar (although not identical), except for the flow direction. The various parameters describing the simulations are listed in Table 1 where we give the values of the physical quantities in computational units, as well as the non-dimensional numbers governing the run. In addition, we give the parameters for a third case with relatively low Reynolds number bubbles in upflow. That case will be discussed at the end of this section. The computational domain is periodic in the direction perpendicular to the walls and in the flow direction. To keep the cost of the computations as low as possible, we use a domain whose thickness is small ($2.5\times d_b$) compared to its width ($W=10\times d_b$), and that is relatively short ($0.75\times W$ for the upflow and $0.8\times W$ for the downflow). The resolution used is shown in Table 1. We have also taken the bubble density to be one-tenth of the liquid

density, again to reduce the computational cost. As discussed in Bunner and Tryggvason (2002), we expect this approximation to have a relatively minor influence on the results. The bubble diameter is 0.2. For the upflow we use 44 bubbles, giving an average void fraction of $\varepsilon_{av} = 0.12287$ and for the downflow we use 40 bubbles, resulting in $\varepsilon_{av} = 0.1047$. For the upflow $-\beta/g\Delta\rho = 0.032$, which is much smaller than the average void fraction, so there is no danger that the core region will be depleted of bubbles. For the upflow the void fraction in the center of the channel, as predicted by Eq. (3) should be $\varepsilon_c = 0.07615$, corresponding to slightly less than 22 bubbles in the center. For the downflow the model predicts that the core void fraction should be $\varepsilon_c = 0.13672$, the thickness of the bubble free wall-layer should be $\delta = 0.2341$ (Eq. (4)), and the downward liquid velocity in the center should be $U_c = -0.3511$, giving a net liquid volumetric downflow of $Q = -0.2869$.

For the present study we are only interested in the steady state behavior and since the transient is fairly long, we have started the simulations using a bubble distribution and an initial liquid velocity that is close to the steady state. For the downflow, where the analytical model gives both a bubble distribution and a velocity profile, this is relatively straight forward, but for the upflow we adjusted the velocity profile a few times by multiplying it by a constant selected to drive it toward a state where Eq. (10) was satisfied. The results presented below were obtained after the systems had reached an approximate steady state.

The bubble distribution at one time, after the flow has reached an approximately statistically steady state is shown in Fig. 2, for upflow on the left and downflow on the right. Isocontours of the vertical velocity in a plane through the middle of the domain are also shown. It is clear that the bubble distribution is very different. For the upflow, about half the bubbles are hugging the walls and most of the bubbles left in the middle of the channel form horizontal clusters. While the bubbles in the center of the channel are clearly spherical, the bubbles near the wall are deformed slightly. For the downflow, there is a bubble free zone near the walls and the distribution of bubbles in the center of the channel is relatively uniform, although it is possible to identify some tendency to form horizontal clusters. The velocity in both cases changes rapidly near the walls, but is relatively uniform in the center. Since the bubbles are rising relative to the liquid, the velocity contours show the wakes of some of the bubbles. Although we show the bubble distribution only at a single instance for each case, we have examined it at several other times and generally find that it is similar to what is shown here, with the exception that the horizontal rafts seen for the upflow are often less prominent. Horizontal clustering of buoyant bubbles, as seen here, was initially predicted by Sangani and Didwania (1993) and Smereka (1993), who assumed potential flow. At finite Reynolds numbers the clustering is generally transient and the clusters are smaller than the potential flow results suggested. For details see the recent experiments of Figueroa-Espinoza and Zenit (2005) and the computations of Esmaeeli and Tryggvason (2005).

In Fig. 3 we plot the horizontal (or cross-channel) coordinate of the bubble centers versus time for both the upflow (left) and the downflow (right) after the flow has reached an approximately steady state. For both cases it is clear that the bubbles interact strongly, although the void fraction in the center is higher in the downflow. In the upflow several bubbles slide along the walls. Their centers are about one bubble radius from the wall and their trajectories are essentially straight. A few bubbles move in and out of the wall-layer, but only rarely.

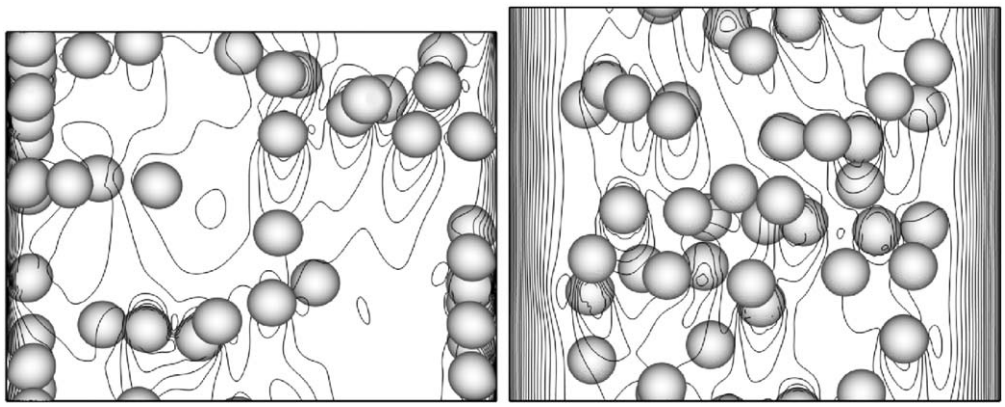

Fig. 2. The bubble distribution and isocontours of the vertical velocity in the middle plane for upflow on the left and dowflow on the right.

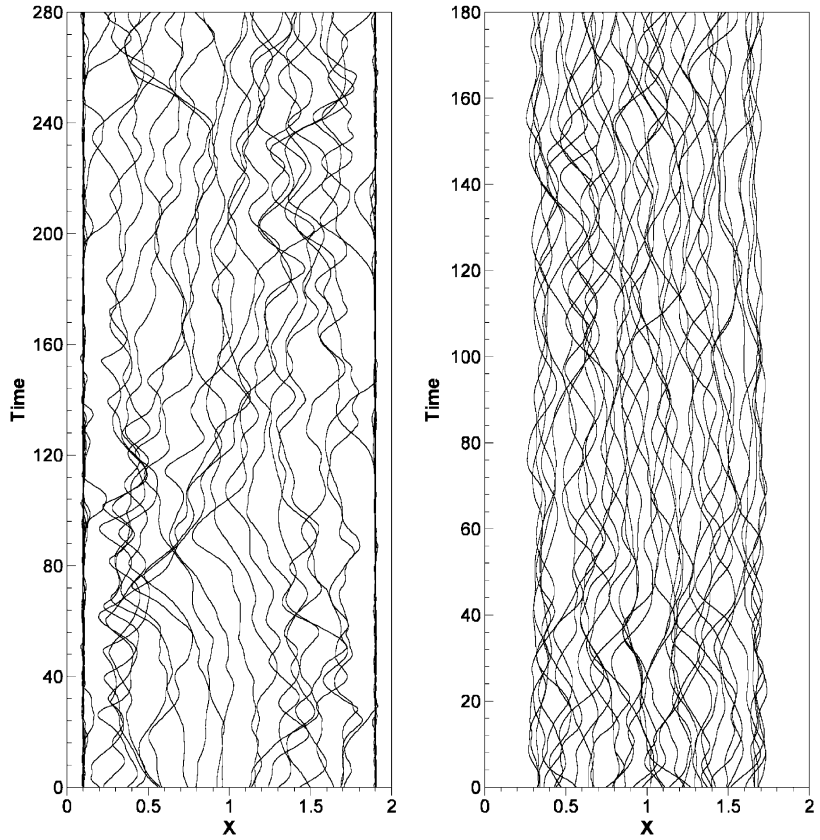

Fig. 3. The path of bubbles. The cross-channel coordinate versus time for the upflow (left) and the downflow (right) after the flow has reached an approximate steady state.

For the downflow, the regions near the walls remain completely free of bubbles and in no case does a bubble center come closer to the wall than about three bubble radii. While bubbles in the downflow seem to be repelled gently if they move close to the bubble free wall-regions, upflow bubbles that belong to the outer edge of the core region seem to bump away more abruptly when they collide with bubbles in the wall-layer.

To assess how well the motion has converged to a steady state, we plot the wall shear stress, averaged over both walls, versus time in Fig. 4(a). The wall shear must be balanced exactly by β—the pressure gradient and the weight of the mixture—at steady state, and the theoretical value (Eq. (10)) is shown by a horizontal dashed line. In both cases does the shear stress match the predicted value. While the downflow wall shear is essentially constant, the shear stress for the upflow exhibits both short and long scale fluctuations as the bubbles interact and bubbles move in and out of the wall-layer. We note, in particular, that while the shear is slightly above the steady state value initially, the expulsion of two bubbles from the wall-layer at just before time 190 (see Fig. 3(left)) coincides with the slight reduction in the wall shear seen in Fig. 4(a) at the same time. The mixture flow rate versus time, for both the up and the downflow is plotted in Fig. 4(b). The flow rate is found by integrating the vertical velocity over the whole computational domain and dividing by the cross sectional area of the domain. While the downflow rate is essentially constant, the upflow flow rate varies slightly and, in particular, the slight downward trend when the wall shear is too high during the early part of the simulation is abruptly reversed when two bubbles are pushed out of the wall-layer. We note that we have run the upflow case for a longer time and found that the slow variations shown here seem to be typical. For convenience we have used the total flow rate here to monitor the convergence. The model in Section 2, however, predicts the liquid flow rate for the downflow, given by Eq. (8). The predicted and the computed liquid flow rate will be compared below, after we present the average relative rise velocity of the bubbles.

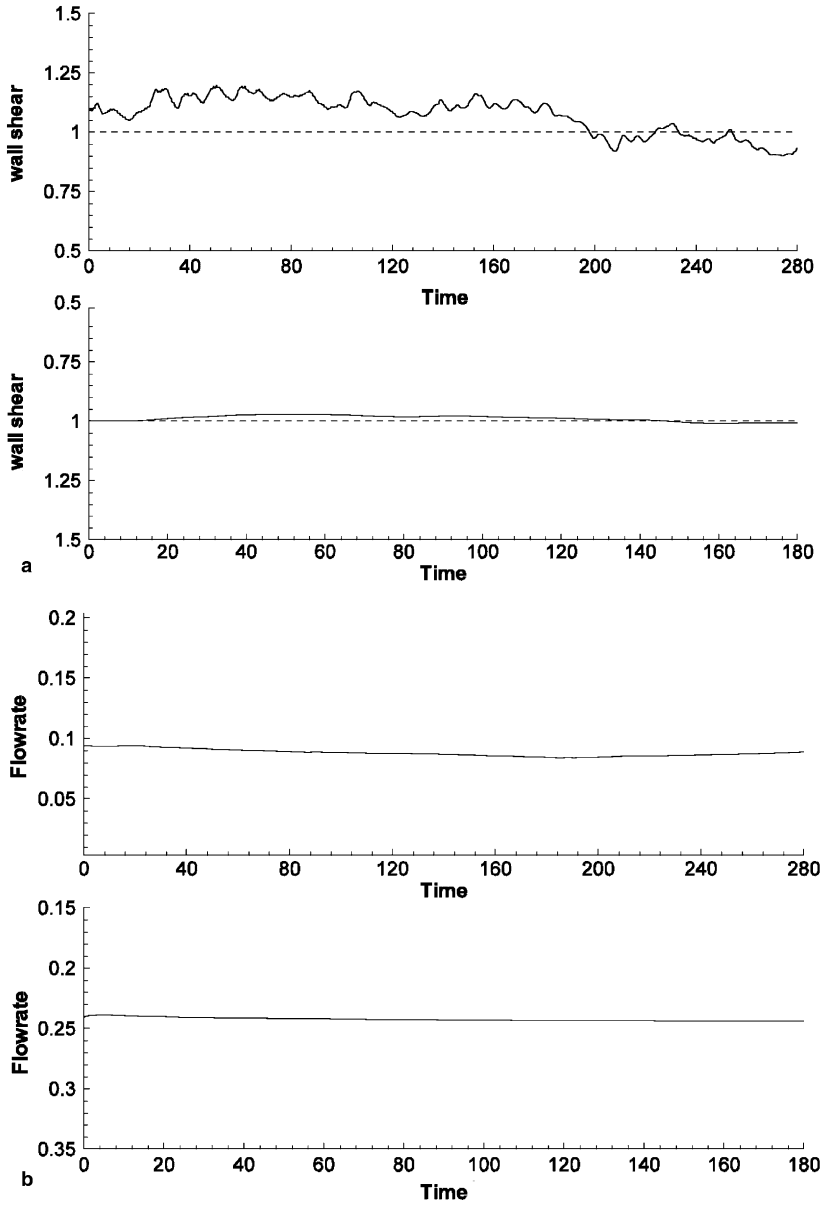

Fig. 4. (a) The averaged wall shear stress versus time for the upflow (top) and the downflow (bottom). The dashed lines represent the corresponding ideal wall shear stress needed to balance the pressure gradient. (b) The total flowrate (liquid and air) versus time for the upflow (top) and the downflow (bottom).

At steady state, the void fraction distribution is predicted by the analysis presented in Section 2, for both the upflow and the downflow. Fig. 5 shows the average void fraction profile across the channel from the simulations, computed by averaging first over planes parallel to the walls and then over several times. Since the domain is relatively small and simulated time is short, we have also averaged the left and the right hand side, forcing the profile to be symmetric. The theoretical predictions are shown by the dashed lines. While the computed profiles exhibit some fluctuations due to the relatively small number of bubbles, and the transition from zero void fraction near the walls for the downflow to the constant void fraction in the center is not as sharp as predicted by the model, the agreement is very good. For upflow the shape of the void fraction profile in the wall-layer is determined by the shape of the bubbles, but the averages are in good agreement. The average void

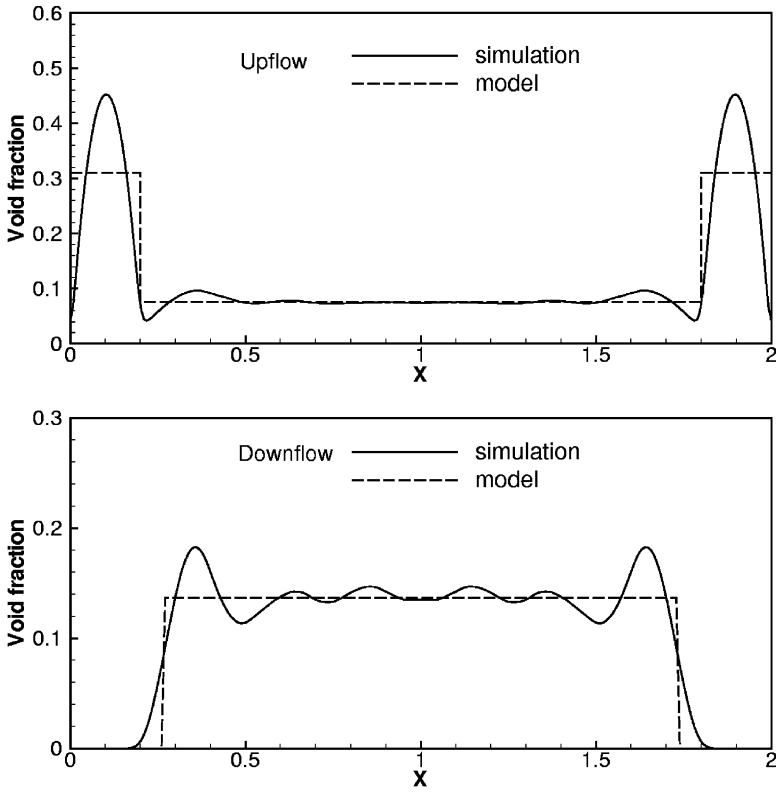

Fig. 5. The average void fraction profile across the channel for the upflow (top) and the downflow (bottom). The solid lines denote the results from the simulations and the dashed lines are the analytical results.

fraction in the wall-layer, predicted to be $\varepsilon_w = 0.3098$, is about half of the void fraction due to a layer of closely packed spheres on the wall (given by $\pi/\sqrt{27} \approx 0.605$).

In Fig. 6 we plot the liquid velocity (the velocity multiplied by an indicator function set to unity in the liquid and zero in the bubble), averaged over planes parallel to the walls, versus the cross-stream coordinate, at one time for the downflow and two times for the upflow. We also show the velocities of all the bubbles in the domain as open circles. For the downflow the liquid velocity is relatively symmetric and uniform in the middle and the bubble velocities are similar. For the upflow the liquid velocity profile is more asymmetric and there is a significant difference between the two times shown. The bubble velocities also exhibit significantly larger fluctuations than for the downflow case.

The average vertical liquid velocity, averaged over time in the same way as the void fraction in Fig. 5, is shown in Fig. 7. For the downflow the model gives the complete velocity profile. The theoretical value is shown by a dashed line and it is clear that the overall agreement is good. For the upflow the model only predicts that the velocity in the center is constant and this is reproduced by the simulation. In Fig. 7 we have also plotted the average bubble velocity, found by dividing the width of the channel into ten equal bins and averaging the bubble velocity in each bin. For the upflow the first and the last bin contain the bubbles in the wall-layer, but for the downflow those bins are empty. The average slip velocity of all the bubbles in the downflow is essentially constant and equal to 0.05313. Similarly, the slip velocity in the core of the upflow channel is equal to 0.05085. The bubbles hugging the wall, on the other hand, are slowed down significantly and the slip velocity has also been reduced significantly. Since the flow in the middle is essentially homogeneous it is natural to compare the bubble slip velocity to the rise velocity of bubbles in fully periodic domains. Although flows of equal size bubbles in fully periodic domains have been studied extensively by direct numerical simulations (Esmaeeli and Tryggvason, 1998, 1999, 2005; Bunner and Tryggvason, 2002a,b), such simulations have not been done for exactly the parameters used here. We therefore conducted two simulations of homogeneous

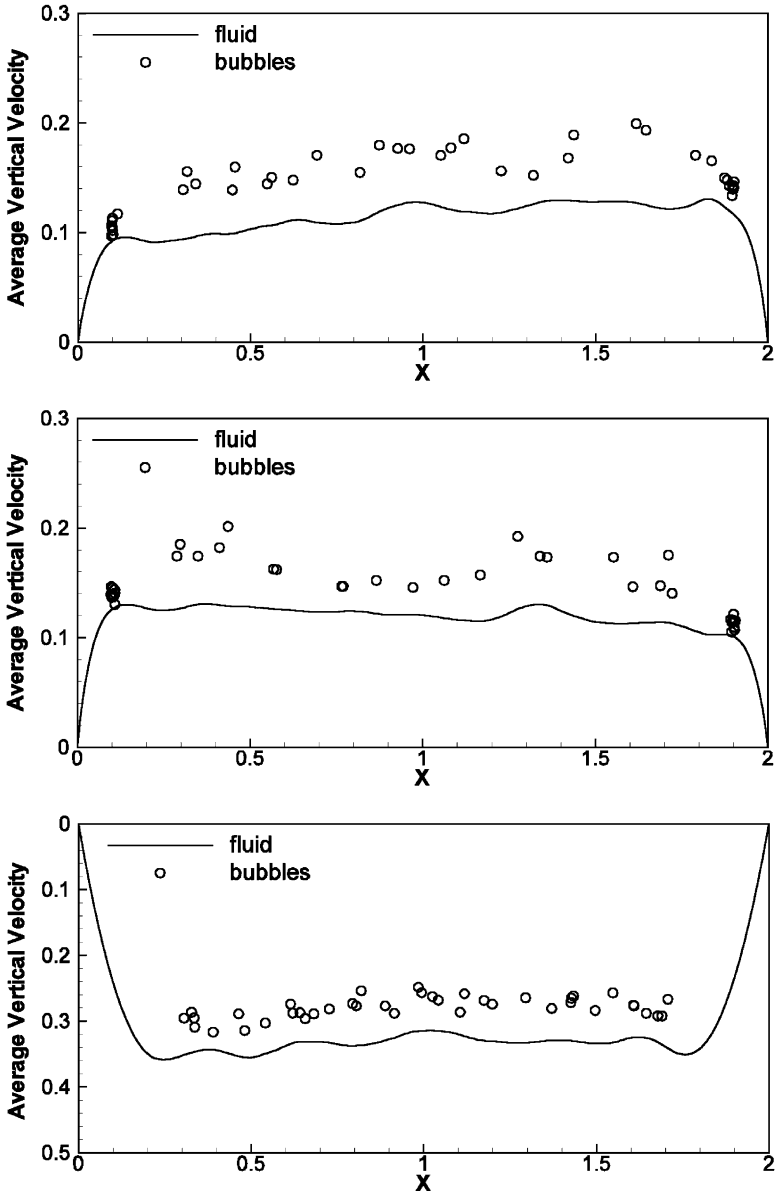

Fig. 6. The average velocity versus the cross channel coordinate at one time for the downflow (bottom) and at two times for the upflow (top and middle). The solid lines denote the fluid velocities, and the circles represent the velocities and the cross-channel coordinates of all the bubbles in the channel.

bubbly flows, but using relatively few bubbles in a small computational domain. As shown by Bunner and Tryggvason (2002) the domain size has a relatively minor influence on the average rise velocity of the bubbles and the statistics that depends primarily on two bubble interactions, such as the velocity fluctuations in the liquid. Using 18 bubbles of diameter 0.2 in a domain of size 0.96^3, giving a void fraction of 0.1364 (equal to the theoretical void fraction in the center of the downflow channel) we found an average slip velocity of 0.0521 (non-dimensionalized in the same way as the channel flow), in good agreement with what we found for the channel. For 18 bubbles in a 1.14 by 1.14 by 0.76 domain and a void fraction of 0.0763, we found an average slip velocity of 0.04314, agreeing reasonably well with what we found for the middle of the upflow channel. The rise velocity of the bubbles in the middle also compares relatively well with experimental correlations for bubbles under similar conditions. Using the formula suggested by Rodrigue (2001) for the terminal

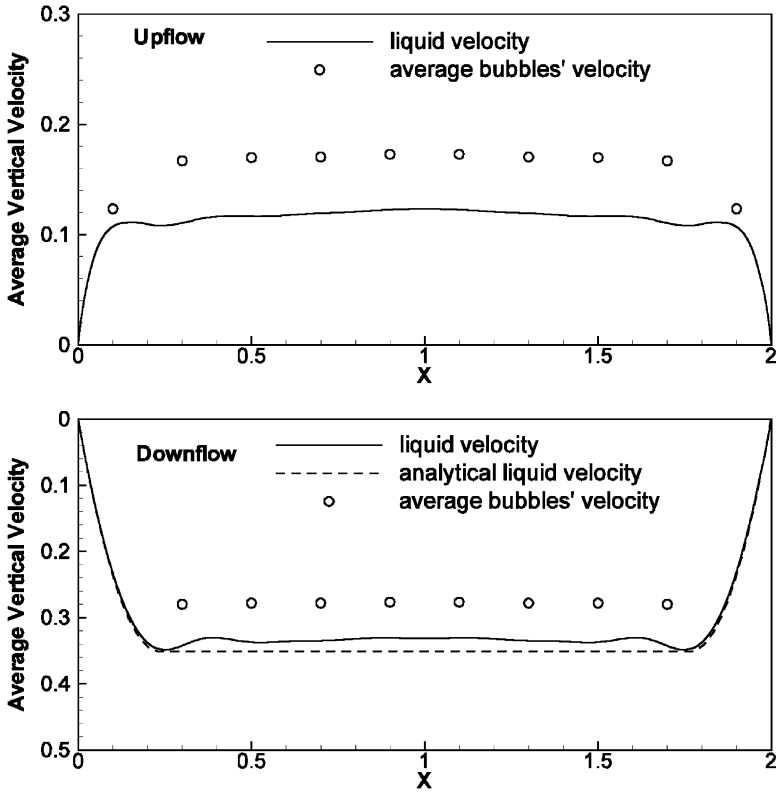

Fig. 7. The average vertical liquid velocity profile across the channel for the upflow (top) and the downflow (bottom). The solid lines are the simulated results, averaged over the time shown in Fig. 3. The dashed line is the analytical results for the downflow. The circles represent the average bubble velocities in 10 equal sized bins across the channel.

velocity of a single bubble in an unbounded fluid and the correlation of Ishii and Zuber (1979) to correct for the effect of a finite void fraction we find that the numerical results for the slip velocity of the bubbles in the periodic domains are about 2.2% higher for the higher void fraction and about 3.2% lower for the lower void fraction. For a more detailed discussion of how the rise velocity of bubbles in full simulations compares with experimental correlations, see Bunner and Tryggvason (2002).

Integrating the average liquid velocity in Fig. 7 for the downflow yields $Q = -0.2755$, as compared with -0.2869 predicted by the model. It is also clear that the computed liquid velocity in the core is about 5% lower than the model prediction. This is most likely due to liquid moving upward with the bubbles. For spherical bubbles in potential flow the drift mass is equal to the added mass (half the mass displaced by the bubble) and by assuming that a volume equal to half the bubble volume is moving by the bubble velocity instead of the predicted liquid velocity, we find that the average downward velocity is reduced by roughly a third of the observed difference. However, using the drift mass for a single isolated bubble in potential flow is obviously an approximation and the finite rise Reynolds number of the bubbles used here (and thus larger wake) is likely to result in a larger drift mass.

We note that the small size of the domain makes the average results relatively sensitive to the details of the flow, particularly for the upflow. If one or two bubbles leave the wall-layer, for example, the flow in the middle of the channel is not completely in hydrostatic equilibrium and we then see a slightly parabolic velocity profile. The averaging period selected here includes times when the number of bubbles in the middle is larger than needed for hydrostatic equilibrium and a careful examination of the velocity profile shows a slight curvature.

The model in Section 2 applies equally well to two-dimensional flows and we have compared the simulation results for downflow presented in Biswas et al. (2005) with the model in Section 2 and found excellent agreement in all cases, both for the averaged velocity and the void fraction profile. As pointed out in Biswas et al.

(2005), the downflow case is insensitive to the exact value of the modeling parameters, as we also conclude from the results presented here.

The bubble distribution and the velocity in the middle of the channel are essentially constant and the slip velocity of the bubbles agrees well with what is found for fully periodic domains. To see if the similarity extends to the unsteady motion of the liquid, we plot the root mean square (rms) velocity fluctuations for both cases in Fig. 8. The averaging is the same as for Figs. 5 and 7. The horizontal lines show the rms velocities from the homogeneous bubby flow simulations. For the downflow the velocity fluctuations are nearly constant in the middle of the channel and relatively well predicted by the results from homogeneous flows, although the channel cross-stream fluctuations, v', are consistently slightly higher. For the upflow the trend is well predicted by the homogeneous flow results, but the quantitative agreement is not as good, particularly for v'. We believe that this is mainly due to the relatively small size of the domain and the persistence of large unsteady asymmetries in the flow and possibly the narrowness of the computational domain.

Another check on the homogeneity of the flow in the middle of the channel comes from looking at the average of the off-diagonal components of the Reynolds stress tensor. In Fig. 9 we plot $\langle u'v' \rangle$ as a function of the cross-channel coordinate, averaged in the same way as for the velocity plots. We have also averaged over the left and the right hand side of the channel, but taking into account that the fluctuations are antisymmetric around the centerline. By symmetry, $\langle u'v' \rangle$ should be exactly zero in homogeneous flows and it is clear in Fig. 9 that for downflow this is true. Near the walls the flow is bubble free and essentially steady so $\langle u'v' \rangle$ is also zero there. For the upflow $\langle u'v' \rangle$ is nearly zero in the center of the channel but we see large fluctuations in a region near the walls that extend about a bubble diameter beyond the wall-layer. We note that while the instantaneous $\langle u'v' \rangle$ profile for the downflow is consistently nearly zero, the profile for the upflow fluctuates

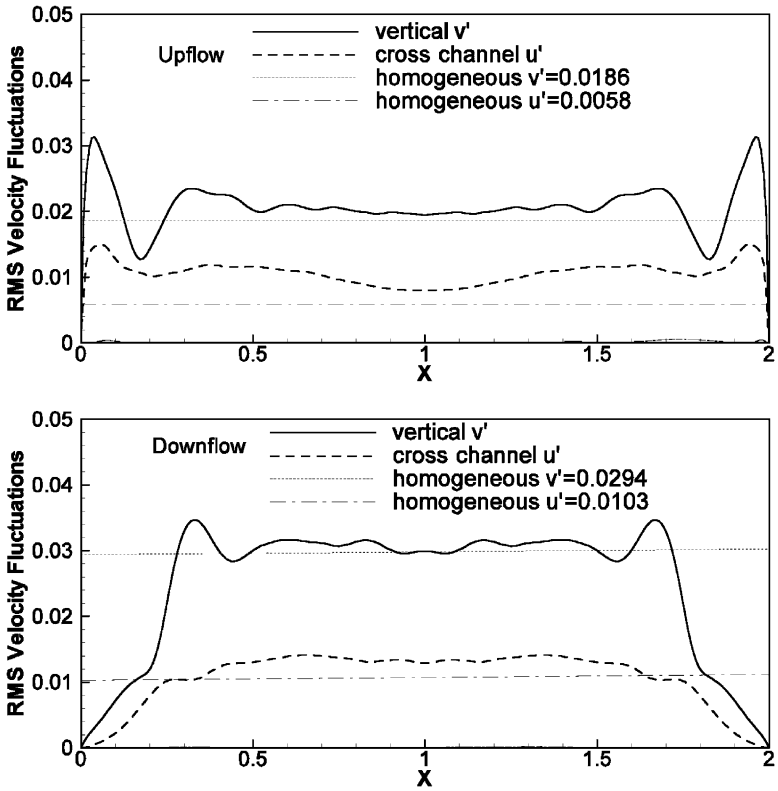

Fig. 8. The root mean square (rms) velocity fluctuations for the upflow (top) and the downflow (bottom). The solid lines are the vertical velocity fluctuations, and the dashed lines are the fluctuations in the cross-channel direction. The dotted and dash–dotted straight lines represent the corresponding velocity fluctuations from homogeneous flow simulations having the same void fraction as predicted theoretically for the center of the channel.

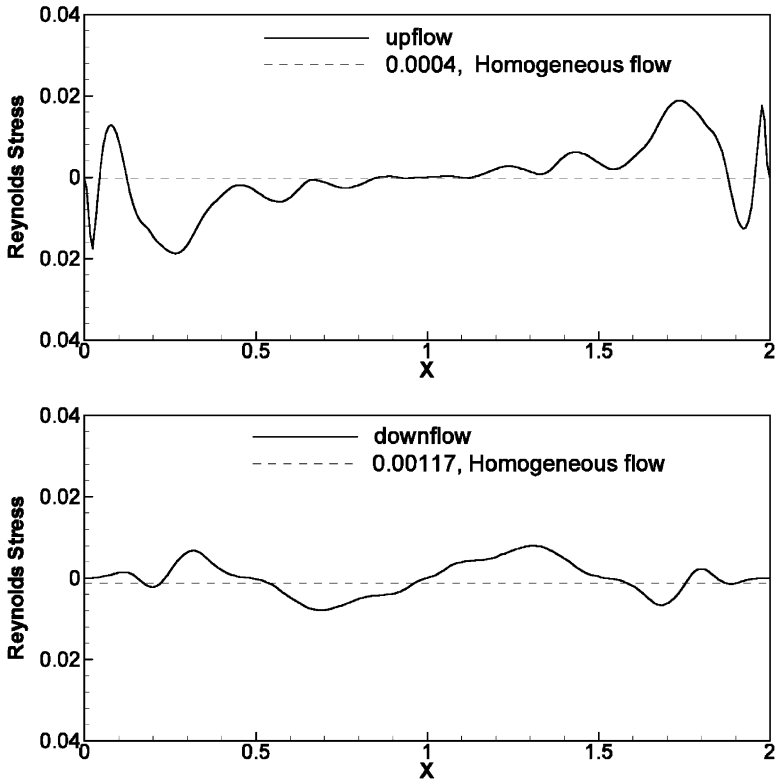

Fig. 9. The average Reynolds stress profile versus the cross-channel coordinate for the upflow (top) and the downflow (bottom). The solid lines are the results of averaging over the time shown in Fig. 3. The dashed lines denote the results form the corresponding homogeneous flow.

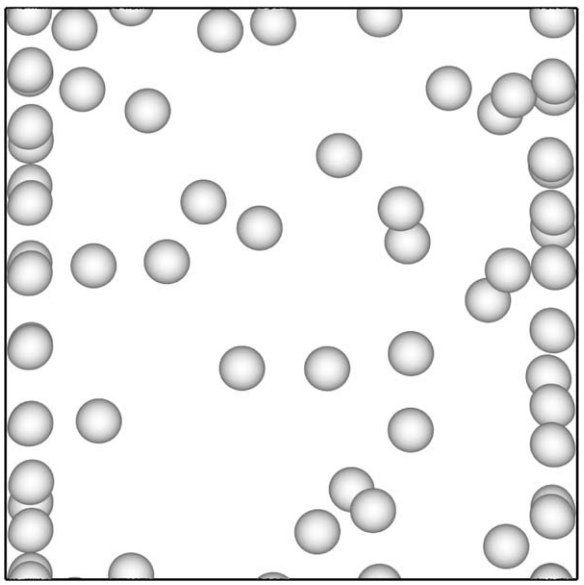

Fig. 10. The bubble distribution at one time for the low Reynolds number upflow case.

much more. Furthermore, since the flow is subject to large asymmetries we would expect to have to take an average over a very long time to get a fully converged profile.

In addition to the two simulations described above, we have conducted one additional study of bubbles in upflow at much lower channel and bubble Reynolds numbers. The various parameters governing the run, along with the relevant non-dimensional numbers are listed in Table 1. We have also carried out a simulation in a fully periodic domain for the void fraction predicted in the middle of the channel. In Fig. 10 the bubble distribution at one late time is shown and the path of the bubbles is shown in Fig. 11. The wall shear and the flow rate are plotted in Fig. 12 along with the theoretical wall-shear, and the average void fraction, velocity profile, velocity fluctuations, and the $\langle u'v' \rangle$ component of the Reynolds stresses are presented in Fig. 13. The average quantities in Fig. 13 are computed in the same way as described earlier, after the flow has reached an approximately steady state, and we include the model predictions for the void fraction in Fig. 13(a) and the results for the homogeneous flow in Fig. 13(c). While the bubble Reynolds number is lower here than for the case considered earlier, the number of bubbles is larger and we have carried the simulation out for a considerably longer time. As a result, all averages are much better converged. The flow rate still shows some long time fluctuations (Fig. 12) but the wall shear is essentially equal to the predicted value. The simulation involves several exchanges of bubbles between the wall-layer and the core (Fig. 11), but the velocity profile is essentially

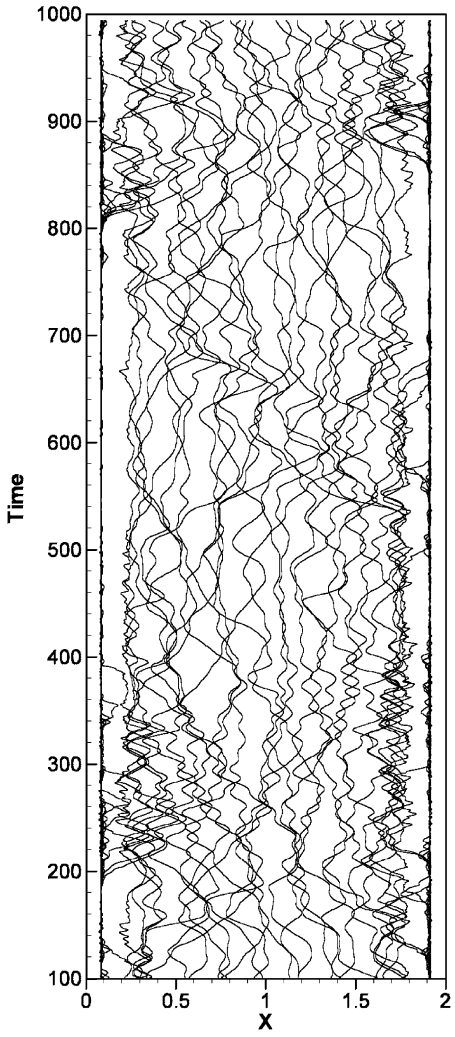

Fig. 11. The cross-channel coordinate of the bubble centers versus time for the low Reynolds number upflow case.

flat (Fig. 13(a)) and the homogeneous region in the middle of the channel is better defined (Fig. 13(d)) although it is clear that the region where $\langle u'v' \rangle$ is non-zero extends beyond the wall-layer. It is also clear that

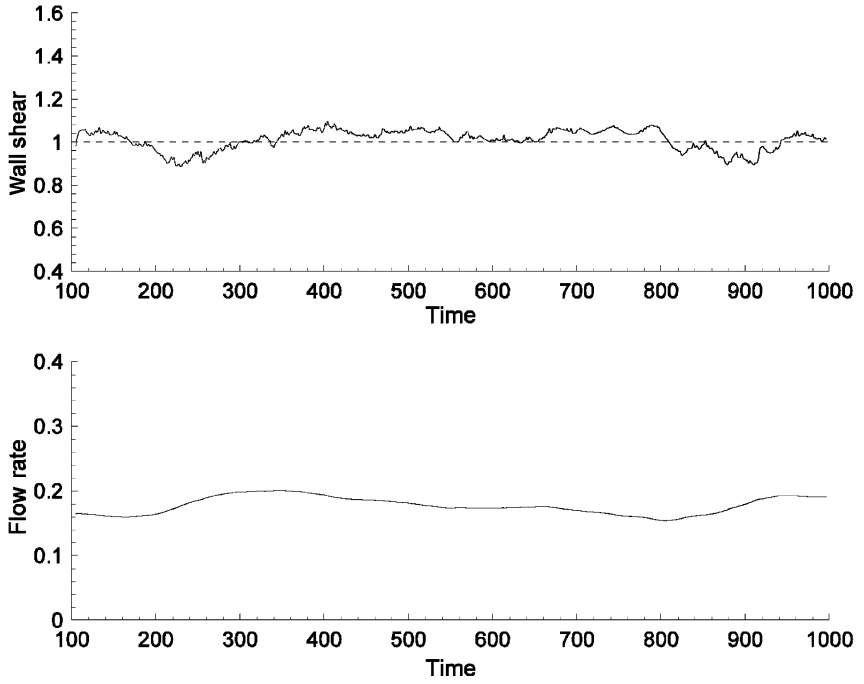

Fig. 12. The wall shear stress (top) and the total flow rate (bottom) versus time for the low Reynolds number upflow.

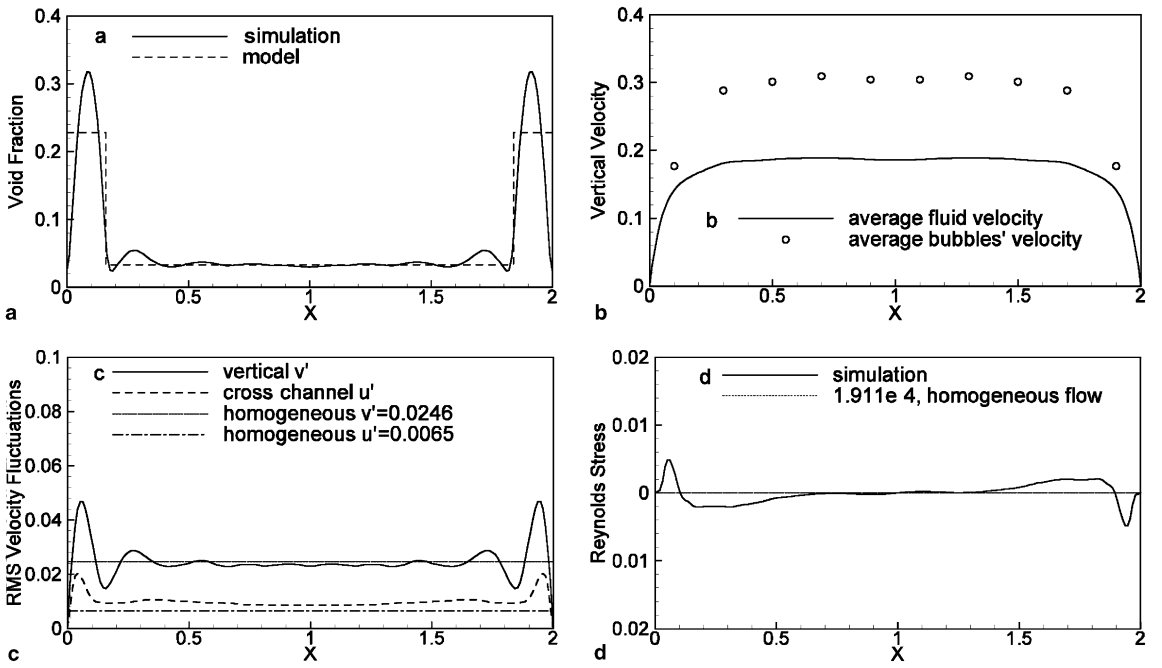

Fig. 13. Average profiles versus the cross-channel coordinate for the low Reynolds number flow. (a) Void fraction, (b) vertical fluid velocity, (c) root mean square velocity fluctuations and (d) shear stress.

while the fluctuation of the streamwise velocity is the same as found in homogeneous flows, the fluctuations of the cross-stream velocity component are slightly larger. We do not have an explanation for this difference as of yet.

5. Conclusions

Direct numerical simulations have been used to examine the statistically steady-state flow of buoyant bubbles in vertical channels. The flow is well described by a simple analytical model and the simulations show that the fundamental assumptions of the model are correct. The flow consists of two regions: A homogeneous region in the middle of the channel—the core region—where the void fraction and the velocity are uniform and a wall-layer that consists of bubbles hugging the wall for upflow but is free of bubbles for downflow. In the core region the weight of the bubble/liquid mixture is balanced exactly by the imposed pressure gradient. The correct void fraction is achieved by pushing bubbles to the wall for upflow and drawing in bubbles from the wall region for downflow. For downflow the thickness of the bubble free wall-layer is determined by the number of bubbles that must be added to bring the core region into hydrostatic equilibrium and for upflow the void fraction of the wall-layer is determined by how many bubbles have to be removed from the core to achieve hydrostatic equilibrium. For downflow, the velocity in the wall-layer can be calculated analytically, but for the upflow the presence of the bubbles makes the flow more complex. For both upflow and downflow the flow rate is governed by the force acting on the wall layer and the core moves by the velocity determined by the wall-layer.

The model says nothing about the motion of the bubbles, but the comparisons done here suggest that results for homogeneous flows, such as those provided by Esmaeeli and Tryggvason (1998, 1999, 2005) and Bunner and Tryggvason (2002a,b), describe the bubbly flow in the channel core reasonably well. For upflow, the model does not specify the dependency of the velocity increase across the wall-layer on the governing parameters. Bubbly wall-layers are commonly observed and So et al. (2002), for example, have looked at some of their properties experimentally. Another study, by Kitagawa et al. (2004), focused on the motion of many bubbles sliding along a (slightly tilted) wall, but the bulk fluid was not moving. Both authors find that the bubbles moving on the wall interact and occasionally seem to form clusters. The small size of our systems did not allow us to see any significant cluster formation.

While the number of cases examined here has been limited, the good agreement with the model predictions suggests that similar results will be obtained for all situations where the bubbles are nearly spherical and of equal size and the flow is laminar. The only exception is upflow where the void fraction is either very low or the pressure gradient high, so all the bubbles end up at the wall. In this case the flow in the center is likely to remain parabolic, but the bubbles in the wall-layer will impose an increase in velocity as seen here. In real systems there are, of course, a few complications. The primary one is the non-uniform size distribution of the bubbles. As long as the bubbles are all nearly spherical it is, however, unlikely that the basic picture seen here will change, although the dynamics of the bubbles both in the core and in the wall-layer will be different. A mixture of small spherical bubbles and large deformable ones is, however, likely to lead to a more complex flow.

The results presented here should be helpful for further development of models for multiphase flows. The two-fluid model of Antal et al. (1991) predicts the hydrostatic balance in the core, as was pointed out by Azpitarte and Buscaglia (2003), but the location of the wall-peak is determined in the model by the relative magnitude of the lift force and the wall-repulsion force. The total through flow is sensitive to the thickness of the wall peak and small changes in the lift force can change the results significantly. Our results suggest, on the other hand, that the steady state is independent of the lift force. The bubbles in the wall-layer hug the wall and the wall-peak is always one bubble radius away from the wall. The presence of a lift force is, however, important in both driving the bubbles to the wall in the first place, as well as keeping them there. While the exact magnitude of the lift may not be important at steady state, its exact value is likely to be important for transient flows. Downflow on the other hand—as observed by several investigators—is insensitive to essentially any modeling parameters. It is, however, important to note that the situation considered here, laminar flow of equal size bubbles, is a limiting case. In practical situations the bubbles are unlikely to be of the same size, they may coalesce and break, they will be contaminated, and the flow is likely to be turbulent. However,

and in the spirit of the study of Antal et al. (1991), we believe that well understood limiting cases must provide the foundation for the modeling of more complex situations.

Acknowledgements

This study was funded by the Department of Energy, Grant DE-FG02-03ER46083. Preliminary computations were done on computers at the Center for Parallel Computing at WPI, but the results reported here were computed using computer time provided by the National Partnership for Advanced Computational Infrastructure, NPACI.

References

Antal, S.P., Lahey Jr., R.T., Flaherty, J.E., 1991. Analysis of phase distribution in fully developed laminar bubbly two-phase flow. Int. J. Multiphase Flow 17, 635–652.

Azpitarte, O.E., Buscaglia, G.C., 2003. Analytical and numerical evaluation of two-fluid model solutions for laminar fully developed bubbly two-phase flows. Chem. Eng. Sci. 58, 3765–3776.

Biswas, S., Esmaeeli, A., Tryggvason, G., 2005. Comparison of results from DNS of bubbly flows with a two-fluid model for two-dimensional laminar flows. Int. J. Multiphase Flow 31, 1036–1048.

Bunner, B., Tryggvason, G., 2002a. Dynamics of homogeneous bubbly flows. Part 1. Rise velocity and microstructure of the bubbles. J. Fluid Mech. 466, 17–52.

Bunner, B., Tryggvason, G., 2002b. Dynamics of homogeneous bubbly flows. Part 2. Fluctuations of the bubbles and the liquid. J. Fluid Mech. 466, 53–84.

Bunner, B., Tryggvason, G., 2003. Effect of bubble deformation on the stability and properties of bubbly flows. J. Fluid Mech. 495, 77–118.

Celik, I., Gel, A., 2002. A new approach in modeling phase distribution in fully developed bubbly pipe flow. Flow Turbul. Combust. 68, 289–311.

Delhay, J.M., 1982. Handbook of multiphase systems. In: Hetsroni, G. (Ed.). Hemisphere- McGraw Hill.

Drew, D.A., Lahey, R.T., 1982. Phase-distribution mechanisms in turbulent low-quality two-phase flow in a circular pipe. J. Fluid Mech. 117, 91–106.

Drew, D.A., Passman, S.L., 1999. Theory of multicomponent fluids. Springer.

Esmaeeli, A., Tryggvason, G., 1998. Direct numerical simulations of bubbly flows. Part I—Low Reynolds number arrays. J. Fluid Mech. 377, 313–345.

Esmaeeli, A., Tryggvason, G., 1999. Direct numerical simulations of bubbly flows. Part II—Moderate Reynolds number arrays. J. Fluid Mech. 385, 325–358.

Esmaeeli, A., Tryggvason, G., 2005. A DNS study of the buoyant rise of bubbles at O(100) Reynolds numbers. Phys. Fluids 17, 093303, 19 pages.

Figueroa-Espinoza, B., Zenit, R., 2005. Clustering in high Re monodispersed bubbly flows. Phys. Fluids 17, 091701.

Guet, S., Ooms, G., Oliemans, R.V.A., Mudde, R.F., 2004. Bubble size effect on low liquid input drift-flux parameters. Chem. Eng. Sci. 59, 3315–3329.

Guet, S., Ooms, G., Oliemans, R.V.A., 2005. Simplified two-fluid model for gas-lift efficiency predictions. AIChE J. 51, 1885–1896.

Ishii, M., Zuber, N., 1979. Drag coefficient and relative velocity in bubbly, droplet or particulate flows. AIChE J. 25, 843–855.

Kashinsky, O.N., Randin, V.V., 1999. Downward bubbly gas–liquid flow in a vertical pipe. Int. J. Multiphase Flow 25, 109–138.

Kataoka, I., Serizawa, A., 1989. Basic equations of turbulence in gas liquid two-phase flow. Int. J. Multiphase Flow 12, 745–758.

Kitagawa, A., Sugiyama, K., Murai, Y., 2004. Experimental detection of bubble–bubble interactions in a wall-sliding bubble swarm. Int. J. Multiphase Flow 30, 1213–1234.

Kuo, T.C., Pan, C., Chieng, C.C., 1997. Eulerian–Lagrangian Computations on phase distribution of two-phase bubbly flows. Int. J. Numer. Meth. Fluids 24, 579–593.

Liu, T.-J., 1997. Investigation of the wall shear stress in vertical bubbly flow under different bubble size conditions. Int. J. Multiphase Flow 23, 1085–1109.

Liu, T.-J., Bankoff, S.G., 1993. Structure of air–water bubbly flow invertical pipe. Part II. Int. J. Heat Mass Transfer 36, 1049–1060.

Lopez-De-Bertodano, M., Lahey Jr., R.T., Jones, O.C., 1987. Development of a k–ε model for bubbly two-phase flow. J. Fluids Eng. 13, 327–343.

Lopez-De-Bertodano, M., Lahey Jr., R.T., Jones, O.C., 1994. Phase distribution in bubbly two-phase flows in vertical ducts. Int. J. Multiphase Flow 20, 805–818.

Lu, J., Fernandez, A., Tryggvason, G., 2005. The effect of bubbles on the wall shear in a turbulent channel flow. Phys. Fluids 17, 095102 (12 pp.).

Luo, R., Pan, X.H., Yang, X.Y., 2003. Laminar light particle and liquid two-phase flows in a vertical pipe. Int. J. Multiphase Flow 29, 603–620.

Matos, A., de Rosa, E.S., Franca, F.A., 2004. The phase distribution of upward co-current bubbly flows in a vertical square channel. J. Braz. Soc. Mech. Sci. Eng. 26, 308–316.

Nakoryakov, V.E., Kashinsky, O.N., Randin, V.V., Timkin, L.S., 1981. Gas liquid bubbly flows in vertical pipes. Int. J. Multiphase Flow 7, 63–81.

Nakoryakov, V.E., Kashinsky, O.N., Randin, V.V., Timkin, L.S., 1996. Gas–liquid bubbly flow in vertical pipes. J. Fluids Eng. 118, 377–382.

Politano, M.S., Carrica, P.M., Converti, J., 2003. A model for turbulent polydisperse two-phase flow in vertical channel. Int. J. Multiphase Flow 29, 1153–1182.

Rodrigue, D., 2001. Generalized correlation for bubble motion. AIChE J. 47, 39–44.

Sangani, A.S., Didwania, A.K., 1993. Dynamics simulations of flows of bubbly liquids at large Reynolds numbers. J. Fluid Mech. 250, 307–337.

Serizawa, A., Kataoka, I., Michiyoshi, I., 1975a. Turbulence structure of air–water bubbly flow. II Local properties. Int. J. Multiphase Flow 2, 235–246.

Serizawa, A., Kataoka, I., Michiyoshi, I., 1975b. Turbulence structure of air–water bubbly flow. III Transport properties. Int. J. Multiphase Flow 2, 247–259.

Sirignano, W.A., 2005. Volume averaging for the analysis of turbulent spray flows. Int. J. Multiphase Flow 31, 675–705.

Smereka, P., 1993. On the motion of bubbles in a periodic box. J. Fluid Mech. 254, 79–112.

So, S., Morikita, H., Takagi, S., Matsumoto, Y., 2002. Laser Doppler velocimetry measurement of turbulent bubbly channel flow. Exp. Fluids 33, 135–142.

Song, Q., Luo, R., Yang, X.Y., Wang, Z., 2001. Phase distributions for upward laminar dilute bubbly flows with non-uniform bubble sizes in a vertical pipe. Int. J. Multiphase Flow 27, 379–390.

Tryggvason, G., Bunner, B., Esmaeeli, A., Juric, D., Al-Rawahi, N., Tauber, W., Han, J., Nas, S., Jan, Y.-J., 2001. A front tracking method for the computations of multiphase flow. J. Comput. Phys. 169, 708–759.

Unverdi, S.O., Tryggvason, G., 1992. A front tracking method for viscous incompressible flows. J. Comput. Phys. 100, 25–37.

Wang, S.K., Lee, S.J., Jones Jr., O.C., Lahey, R.T., 1987. 3-D turbulence structure and phase. Distribution measurements in bubbly two-phase flows. Int. J. Multiphase Flow 13, 327–343.

Zhang, D.Z., Prosperetti, A., 1994. Averaged equations for inviscid disperse two-phase flow. J. Fluid Mech. 267, 185–219.